A Comparison of Model Predictive Control Schemes for MV Induction Motor Drives

James Scoltock, *Student Member, IEEE,* Tobias Geyer, *Senior Member, IEEE,* and
Udaya K. Madawala, *Senior Member, IEEE*

Abstract—In Medium-Voltage (MV) drives, the switching frequency is limited to a few hundred Hz, for which high-performance control and modulation schemes are necessary to maintain acceptable current and torque distortion. Forced Machine Current Control (FMCC) is a predictive control strategy for MV drives which was proposed in the early 1980s, which can be formulated for either torque or current control. Recently, Model Predictive Direct Torque Control (MPDTC) and Model Predictive Direct Current Control (MPDCC) have been developed, sharing with FMCC the use of hysteresis bounds, switching and prediction horizons. However, the relative performances of these schemes are yet to be compared. Through simulation, this paper compares the schemes across a range of operating points. It is shown that the steady state performance of MPDxC and FMCC is similar when the switching horizon of MPDxC is limited. However, when the switching horizon is extended, the performance of MPDxC is shown to be superior to FMCC, the horizon of which is inherently restricted.

Index Terms—Current control, medium-voltage drives, model predictive control, torque control

I. INTRODUCTION

IN recent years, the Model Predictive Control (MPC) concept has received significant attention from the power electronics and drives community. MPC, which was developed for process control in the 1970's [1], is used widely in industry, with numerous applications reported [2]. Within the electrical drives field, two main subcategories of MPC have emerged. The first extends on traditional Field-Oriented Control (FOC) by replacing the inner current control loop with an MPC-based controller while retaining a modulator. Such strategies are discussed in [3] and [4]. The second discards a modulator altogether, with MPC directly manipulating the inverter switch positions, as discussed in [5] - [8]. Model Predictive Direct Torque Control (MPDTC), which emerged several years ago, is a variant of MPC and an extension of Direct Torque Control (DTC), as it replaces the look-up table of DTC with an online-optimisation process in the control of machine torque and flux [5] - [7]. MPDTC has shown significant promise in the control of MV drives and has been experimentally verified at

J. Scoltock and U.K. Madawala are with the Department of Electrical and Computer Engineering, The University of Auckland, 1052 Auckland, New Zealand (email: jsco075@aucklanduni.ac.nz, u.madawala@auckland.ac.nz).

T. Geyer is with ABB Corporate Research, 5405 Baden-Dättwil, Switzerland (email: t.geyer@ieee.org).

power levels in excess of 1 MW [8]. Model Predictive Direct Current Control (MPDCC) is a more recent variant of MPC which treats the machine's stator currents as the variables to be controlled [9] - [11]. Numerous other predictive control schemes have also been developed, notably the predictive current [12] - [15] and torque [14] - [16] schemes proposed by Rodriguez *et al*.

Although MPC has only recently become popular in the field of power electronics, predictive control schemes for AC motor drives have been proposed since the early 1980s. In particular, the hysteretic Forced Machine Current Control (FMCC) schemes proposed by Holtz and Stadtfeld in [17] - [19], and Khambadkone and Holtz in [20], share a number of similarities with modern MPDxC. As proposed in [18] and [20], FMCC with a Rectangular Boundary (FMCC-R) shares with MPDTC the ability to directly control the motor's electromagnetic torque distortion. FMCC with a Circular Boundary (FMCC-C), as proposed in [17] and [19], is more akin to MPDCC, with the controller aiming to minimise stator current distortion. However, the most significant similarity between FMCC and MPDxC is the use of a switching and prediction horizon. By utilising the concept of extrapolation, both schemes are able to achieve prediction horizons in the range of tens of time-steps with short switching horizons.

MPDxC schemes have been extensively compared with carrier-based Pulse Width Modulation (PWM), Space Vector Modulation (SVM) and Optimised Pulse Patterns (OPP) [10]. However, a review and comparison of MPDxC against FMCC has never been carried out. Such a comparison is useful, as it gives a clear insight into the advantages of the modern schemes, relative to early predictive control techniques. Although they are gaining popularity, the modern MPC-based schemes are computationally intensive, especially as switching and prediction horizons are lengthened. This necessitates powerful control hardware, although the investigation of efficient mathematical techniques, notably branch and bound, has been shown to reduce the computational effort by an order of magnitude [21]. In contrast, when FMCC was proposed, the computational resources which were available were very limited, and as such the computational burden of FMCC is modest.

The aim of this paper is, therefore, to describe and benchmark the modern MPDxC schemes against FMCC. Although FMCC has been mentioned in survey papers [14], it has not been examined analytically nor has its performance been benchmarked against other predictive schemes since it was ini-
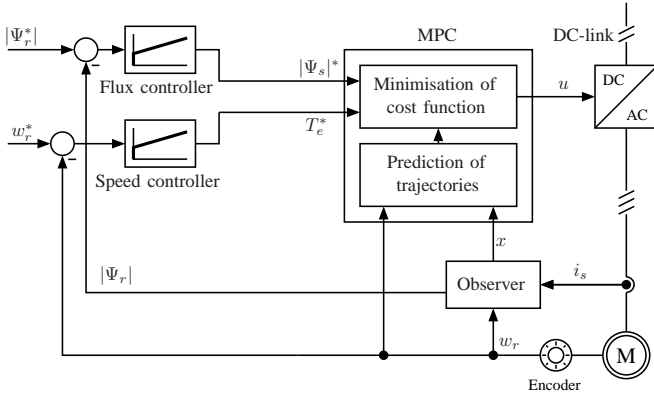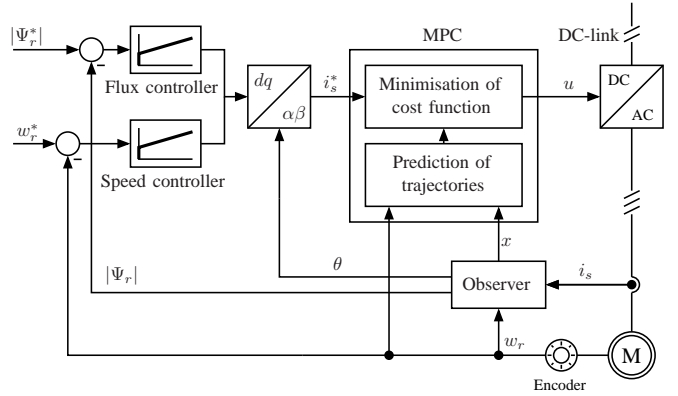
Fig. 1: A predictive torque-control setup.

Fig. 2: A predictive current-control setup.

tially proposed. As such, the similarities between the hysteresis bounds and control procedures of MPDTC and FMCC-R, and MPDCC and FMCC-C, have been investigated. The trade off between switching frequency and current/torque distortion is a fundamental principle to power converters and forms the basis of performance evaluation, with both stator current and electromagnetic torque distortion presented as trade-off curves against switching frequency. The schemes will be compared through a MATLAB-based drive-system simulation which consists of a three-level, Neutral Point Clamped (NPC) Voltage Source Inverter (VSI) driving a squirrel-cage Induction Motor (IM).

The structure of the paper is as follows. Section II summarises the physical model of the drive and formulates the model into a form which can be utilised as an internal model for predictive controllers. Section III discusses the performance criteria which are used throughout the paper. Section IV outlines the MPDxC and FMCC hysteresis bounds and Section V details the control procedures. The relative performance of the schemes is evaluated in Section VI.

A case study for the drive system has been chosen such that the schemes can be compared in a general sense. Non-ideal characteristics of practical drive systems have been ignored to prevent them from obscuring the performance of the control systems in question. The assumptions which have been made regarding the drive system are as follows:

- DC-link: It is assumed that the DC-link acts as a perfect, ripple-free voltage source. Since FMCC was initially proposed for two-level converters, [17] - [20] do not mention neutral point balancing, and as such the neutral point potential is assumed to remain fixed.
- Inverter: Deadtime, turn-on and turn-off times are ignored.
- Electrical machine: The machine's magnetic material is assumed to be linear, ignoring saturation. Skin effect and variations in rotor resistance are ignored.
- Controller: The delay between the sampling instant and the output of the controller is assumed to be negligible.
- Measurements: All measurements are considered to be ideal, and are thus free of noise, offsets and gain errors.
- Load: The mechanical load is constant.

II. DRIVE SYSTEM

A. System Setup

The case-study for the drive system used in this paper utilises an inner and outer control loop, as shown in Figs. 1 and 2. The outer flux and speed regulators are PI controllers which regulate the stator flux, electromagnetic torque or stator current reference values based on the flux and speed references. The outer loop operates in the rotating dq reference frame. The inner predictive loop makes switching decisions based on state feedback and the reference(s) provided by the outer control loop. It is the inner loop which relates to the predictive control schemes described in this paper.

B. Inverter Model

The typical setup for a three-level NPC inverter driving an IM is shown in Fig. 3. Each phase leg is able to assume one of three states, which may be represented by the integer variables $u_a, u_b, u_c \in \{-1, 0, 1\}$. With three voltage levels per phase and three phases, there are $3^3 = 27$ possible switching states of the form $u_{abc} = [u_a \ u_b \ u_c]^T$. Within those states, 19 distinct voltage vectors exist which the inverter is capable of producing. The voltage vectors can be represented by transforming the switching states from the three-phase abc system to the orthogonal $\alpha\beta$ system. This is achieved by using

$$v_{\alpha\beta} = \frac{V_{dc}}{2} P u_{abc} \tag{1}$$

where $v_{\alpha\beta} = [v_\alpha \ v_\beta]^T$, V_{dc} is the DC-link voltage and P is the transformation matrix

$$P = \frac{2}{3} \begin{bmatrix} 1 & -\frac{1}{2} & -\frac{1}{2} \\ 0 & \frac{\sqrt{3}}{2} & -\frac{\sqrt{3}}{2} \end{bmatrix} . \tag{2}$$

In the inverter under consideration all switching transitions are allowed except for those which involve switching between the upper and lower rails. For example, a transition from $u_{abc} = [1 \ 1 \ 1]^T$ to $[0 \ 0 \ 1]^T$ is allowed, whereas a transition to $[-1 \ 1 \ 1]^T$ is not.

C. Induction Machine Model

The IM is modeled in the $\alpha\beta$ reference frame, with the mechanical load assumed to be constant. For both torque and current control, the system state variables are the $\alpha\beta$
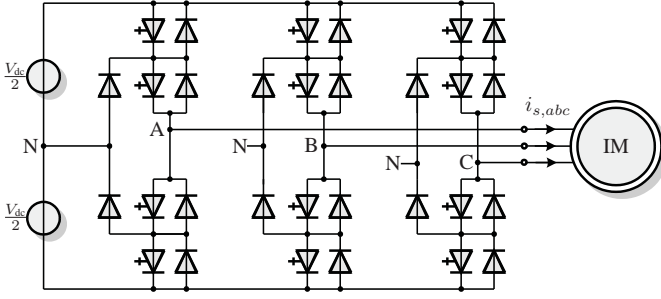
Fig. 3: Three-level neutral point clamped voltage source inverter driving an induction motor.

components of the stator currents and rotor fluxes, $i_{s\alpha}$, $i_{s\beta}$, $\Psi_{r\alpha}$ and $\Psi_{r\beta}$, respectively. The input vector is the three-phase switch position u_{abc}. The model parameters are the angular velocity of the rotor, ω_r, the resistances of the stator and rotor r_s and r_r respectively, the reactances of the stator and rotor x_{ls} and x_{lr} respectively, the mutual reactance x_m, the mechanical inertia of the load, J, and the mechanical torque of the load, T_l. With the state vector of the drive defined as

$$x = [i_{s\alpha} \ i_{s\beta} \ \Psi_{r\alpha} \ \Psi_{r\beta}]^T \tag{3}$$

and the input vector as the three-phase switch position

$$u = [u_a \ u_b \ u_c]^T \in \{-1, 0, 1\}^3 \tag{4}$$

the continuous-time state equation of the system can be defined as [22]

$$\frac{dx}{dt} = Ax + Bu \tag{5}$$

with A being the state matrix

$$A = \begin{bmatrix} -\frac{1}{\tau'_\sigma} & 0 & \frac{k_r}{r_\sigma \tau_r \tau'_\sigma} & \frac{k_r \omega_r}{r_\sigma \tau'_\sigma} \\ 0 & -\frac{1}{\tau'_\sigma} & -\frac{k_r \omega_r}{r_\sigma \tau'_\sigma} & \frac{k_r}{r_\sigma \tau_r \tau'_\sigma} \\ \frac{x_m}{\tau_r} & 0 & -\frac{1}{\tau_r} & -\omega_r \\ 0 & \frac{x_m}{\tau_r} & \omega_r & -\frac{1}{\tau_r} \end{bmatrix} \tag{6}$$

and B the input matrix

$$B = \begin{bmatrix} \frac{1}{r_\sigma \tau_{\sigma'}} & 0 & 0 & 0 \\ 0 & \frac{1}{r_\sigma \tau_{\sigma'}} & 0 & 0 \end{bmatrix}^T \frac{V_{dc}}{2} P. \tag{7}$$

The electromagnetic torque, T_e, is given by

$$T_e = \frac{3}{2} k_r (i_{s\beta} \Psi_{r\alpha} - i_{s\alpha} \Psi_{r\beta}) \tag{8}$$

and the relationship between rotor speed and torque is given by

$$\frac{d\omega_r}{dt} = \frac{1}{J}(T_e - T_l). \tag{9}$$

The deduced parameters used in the above equations are the rotor coupling factor $k_r = x_m/x_r$, total leakage factor $\sigma = 1 - x_m^2/x_s x_r$, leakage reactance $x_\sigma = \sigma x_s$, where $x_s = x_{ls} + x_m$ and $x_r = x_{lr} + x_m$, and equivalent resistance $r_\sigma = r_s + k_r^2 r_r$. The deduced time constants include the transient stator time constant $\tau'_\sigma = x_\sigma/r_\sigma$, and the rotor time constant $\tau_r = x_r/r_r$. Equations (3) – (9) provide a complete description

of the dynamic behaviour of the IM when non-idealities such as magnetic saturation, the skin effect and variations in the rotor resistance are ignored.

D. Internal Control Model

In order for a predictive control scheme to be implemented, a discrete-time model of the drive is required to serve as an internal prediction model for the controller. The model's purpose is to predict the trajectory of the state variables over as many sampling intervals as are required. Due to the fact that the rotor time constant greatly exceeds the length of a prediction horizon, the rotor speed is assumed to be constant within the prediction horizon and is treated as a model parameter rather than an additional variable [7], [9]. From the continuous-time state equation of (3) – (7), the following discrete-time state equation can be derived

$$x(k+1) = (I + T_s A)x(k) + T_s Bu(k) \tag{10}$$

where I is the 4x4 identity matrix and T_s is the sampling time of 25μs.

The output equation depends on the exact definition of the output variables. For MPDTC, the output variables are the electromagnetic torque, T_e, and the stator flux magnitude, $|\Psi_s|$. With the output vector defined as

$$y = [T_e \ |\Psi_s|]^T \tag{11}$$

we can define the discrete-time output equation as

$$y(k) = g(x(k)) \tag{12}$$

where $g(x(k))$ is given by

$$g(x(k)) = \left[\begin{array}{c} \frac{3}{2} k_r (x_1(k) x_3(k) - x_2(k) x_4(k)) \\ \sqrt{(x_\sigma x_1(k) + k_r x_3(k))^2 + (x_\sigma x_2(k) + k_r x_4(k))^2} \end{array} \right]. \tag{13}$$

With the output vector composed of the $\alpha\beta$ stator currents, as is the case for MPDCC and FMCC, the output vector is defined as

$$y = [i_{s\alpha} \ i_{s\beta}]^T \tag{14}$$

with the output defined as

$$y(k) = Cx(k) \tag{15}$$

where C is given by

$$C = \begin{bmatrix} 1 & 0 & 0 & 0 \\ 0 & 1 & 0 & 0 \end{bmatrix}. \tag{16}$$

III. PERFORMANCE CRITERIA

In evaluating the quality of the control and modulation scheme of a drive system, two of the most important factors to consider under steady-state operation are the inverter switching losses and the electromagnetic torque and stator current distortion. Criteria relating to transient response and the robustness of the controller can also be examined, however since this paper focuses on performance under steady state conditions, these have not been considered.
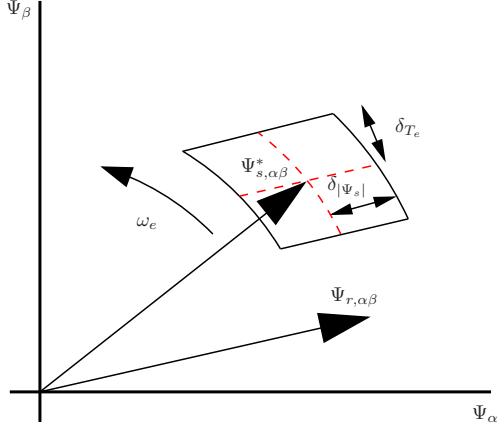
Fig. 4: Hysteresis bounds for MPDTC in terms of stator flux on the $\alpha\beta$-plane.

A. Total Demand Distortion

Total Demand Distortion (TDD) is a suitable measure of the harmonic distortion of the stator current. TDD is defined as

$$I_{TDD} = \frac{\sqrt{0.5 \sum_{h>1} I_h^2}}{I_{nom}} \qquad (17)$$

where I_{nom} refers to the nominal value of the RMS current at full speed and load, while $I_h, h > 1$ refers to the harmonic components of the current, from the second harmonic I_2 to the h-th harmonic component I_h. The harmonic distortion of the electromagnetic torque is similarly defined. TDD is a better measure of distortion than Total Harmonic Distortion (THD) due to the fact that at low levels of current/torque, THD will approach infinity, while TDD will remain relatively constant. In this paper, all harmonic content up to and including 20 kHz is considered when calculating TDD.

B. Switching Losses

The switching losses of an inverter depend on the DC-link voltage, the commutated current, the average switching frequency and the semiconductor characteristics. For MPC, the switching losses can be minimised in two ways. The first is to minimise the losses by minimising the switching frequency. The second is to directly calculate and minimise the losses that are predicted to occur as a result of switching. For an NPC converter the conduction losses are independent of the switching pattern and are, therefore, not relevant in evaluation of the control scheme.
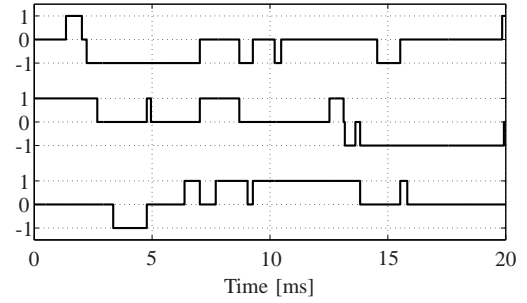
IV. HYSTERESIS BOUNDS

Both MPDxC and FMCC utilise hysteresis bounds around each of the output variables, with the objective of the controllers being to regulate the outputs about their references while minimising switching losses. For both MPDxC and FMCC, the hysteresis bounds act as the primary tuning parameter, setting the trade-off between switching losses and distortion. By narrowing the bounds, the outputs deviate less from their references, resulting in lower distortion but higher switching frequency/losses, and vice versa.
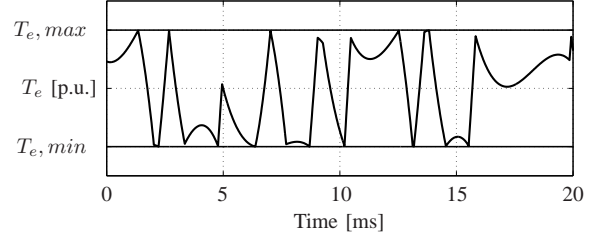
(a) Electromagnetic torque.
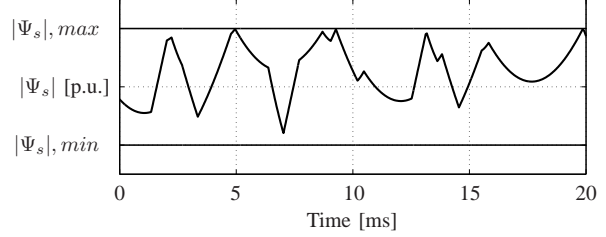
(b) Stator flux magnitude.

(c) Inverter switch positions (top: u_a, middle: u_b, bottom: u_c).

Fig. 5: Simulated output trajectory for MPDTC with torque and flux references of 1 p.u. The hysteresis bounds are $\delta_{T_e} = \pm 0.1$ p.u. and $\delta_{|\Psi_s|} = \pm 0.1$ p.u.

A. Model Predictive Direct Torque Control (MPDTC)

MPDTC utilises hysteresis bounds around the stator flux magnitude, $|\Psi_s|$, and the electromagnetic torque of the motor, T_e. Fig. 4 illustrates the hysteresis bounds as they are defined in terms of the stator flux on the $\alpha\beta$-plane. The dashed, curved line denotes the path of the stator flux reference, $\Psi_{s,\alpha\beta}^*$. The stator flux magnitude is regulated via the radial width of the boundary area, with the difference between the upper (or lower) bound and the stator flux magnitude reference denoted by $\delta_{|\Psi_s|}$. The electromagnetic torque is regulated via the angle between the stator and rotor fluxes, with the difference between the upper (or lower) bound and the torque reference denoted δ_{T_e}. Fig. 5 shows an example output trajectory, along with inverter switch positions, for MPDTC over a period of 20 ms.

Although MPDTC is most naturally formulated in terms of stator flux, it can also be formulated in terms of stator current. The bounds can be expressed in terms of stator current via

$$i_{s,\alpha\beta} = \frac{1}{x_r x_\sigma} \left(\begin{bmatrix} x_r & 0 \\ 0 & x_r \end{bmatrix} \Psi_s - \begin{bmatrix} x_m & 0 \\ 0 & x_m \end{bmatrix} \Psi_r \right) \quad (18)$$

where $i_{s,\alpha\beta} = [i_{s\alpha} \ i_{s\beta}]^T$, $\Psi_s = [\Psi_{s\alpha} \ \Psi_{s\beta}]^T$, and $\Psi_r = [\Psi_{r\alpha} \ \Psi_{r\beta}]^T$. The resulting stator current reference and bound-

ary area is a scaled and shifted version of the boundary depicted in Fig. 4.

MPDTC can also be formulated in the synchronously rotating dq reference frame. The stator current can be transformed from the $\alpha\beta$ plane via

$$i_{s,dq} = Ki_{s,\alpha\beta} \qquad (19)$$

where $i_{s,dq} = [i_{sd} \ i_{sq}]^T$ and K is the transformation matrix

$$K = \begin{bmatrix} cos(\theta) & sin(\theta) \\ -sin(\theta) & cos(\theta) \end{bmatrix} \qquad (20)$$

which results in a stator current reference and boundary area which is fixed in the dq-plane. (Note that the angle θ is aligned with the d-axis of the rotor flux such that the q-axis component of the rotor flux, Ψ_{rq}, is equal to zero). Fig. 6(a) depicts the MPDTC boundary area as defined in terms of stator currents in the dq reference frame, where m denotes the scaling factor of $1/x_\sigma$ which arises in expressing the bounds in terms of stator current.

B. Forced Machine Current Control - Rectangular Boundary (FMCC-R)

FMCC-R, as described in [18], shares with MPDTC the ability to independently control the electromagnetic torque and stator flux (or current) distortion of the machine. The electromagnetic torque of the machine, T_e, is given by

$$T_e = \frac{3}{2}k_r(i_{sq}\Psi_{rd} - i_{sd}\Psi_{rq}) \qquad (21)$$

and by aligning the angle θ with the d-axis of the rotor flux, as described in Sect. IV-A, the torque can be expressed as

$$T_e = \frac{3}{2}k_r(i_{sq}\Psi_{rd}). \qquad (22)$$

With the rotor flux assumed constant, the electromagnetic torque is controlled by the q-axis component of the stator current, i_{sq}. By defining symmetrical hysteresis bounds around each of the d and q-axis stator current components, the torque and current distortion can be controlled with a large degree of independence. Fig. 6(b) illustrates the rectangular boundary area of FMCC-R. The ripple of the q-axis stator current, and therefore electromagnetic torque distortion, is controlled via the height of the boundary, where δ_q denotes the difference between the upper (or lower) q-axis bound and the q-axis stator current reference. The stator current distortion is controlled by both the height and width of the boundary, where δ_d denotes the difference between the upper (or lower) d-axis bound and the d-axis stator current reference.

C. Model Predictive Direct Current Control (MPDCC)

MPDCC utilises symmetrical hysteresis bounds around each of the abc stator current references. δ_i denotes the difference between the upper (or lower) bound and the reference. In order to simplify the problem, MPDCC can be reformulated in the $\alpha\beta$-plane. By transforming the abc hysteresis bounds to the $\alpha\beta$-plane, a hexagonal boundary area centred on the reference current $i_{s,\alpha\beta}^*$ results. The bounds can be further

transformed to the dq-reference plane, which results in a hexagonal boundary area centred on the stationary reference current $i_{s,dq}^*$. Due to the synchronously rotating nature of the dq-plane, the hexagonal boundary is not fixed in space. As shown in Fig. 7(a), the boundary area rotates at synchronous speed ω_e in an anti-clockwise direction.

D. Forced Machine Current Control - Circular Boundary (FMCC-C)

Unlike MPDCC, where the bounds are defined around each of the phase currents separately, FMCC-C as described in [17], instead utilises a radial boundary area directly defined around the stator current reference on the $\alpha\beta$-plane. δ_r denotes the radius of the boundary area. The bounds can be transformed to the dq-plane, which results in a fixed reference current $i_{s,dq}^*$ and boundary area as shown in Fig. 7(b).

V. Control Procedures

Both MPDxC and FMCC replace the inner current control loop and modulator of traditional FOC with a single online-optimisation stage. In doing so, MPDxC and FMCC are able to address the control and modulation problems simultaneously by directly manipulating the switching state of the inverter.

A. Model Predictive Direct Torque/Current Control (MPDxC)

In describing MPDxC it is important to distinguish between the switching horizon, N_s, and prediction horizon, N_p. The switching horizon refers to the number of switching transitions within a prediction, with extension of the output trajectory occurring after each switching event until one or more hysteresis bounds are reached, at which point another switching event takes place. The switching horizon can therefore be defined in terms of the elements 'S' and 'E', for switch and extend respectively. A switching horizon of 'eSESE' is therefore composed of a switching transition, an extension until one or more bounds are reached, a second switching transition, and a second extension until one or more bounds are reached. Note that the lower case 'e' refers to an optional extension leg at the beginning of the switching horizon. The prediction horizon N_p refers to the total number of time-steps into the future for which the prediction is made, which will vary based on the exact switching sequence which is being predicted. The extension of output trajectories gives rise to long prediction horizons of as many as 100 time-steps. Extension steps can be precise, utilising the internal control model, or an approximation, utilising linear or quadratic interpolation or extrapolation [23].

The aim of the controller is to regulate the outputs within their hysteresis bounds while minimising the switching losses of the converter. At each time-step k the set of allowable switching sequences forward in time is determined for the switching horizon N_s based on the current switching state $u(k-1)$. For each sequence, the trajectory of the output variables forward in time is predicted using the internal model of the controller, with only those sequences which remain candidates over the entire prediction considered. A candidate
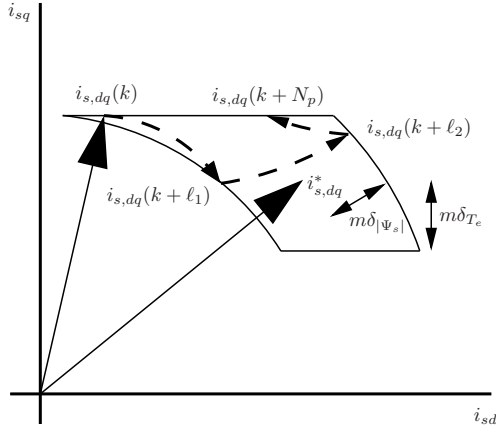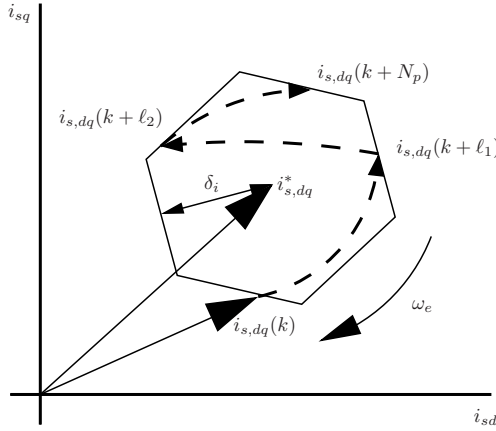
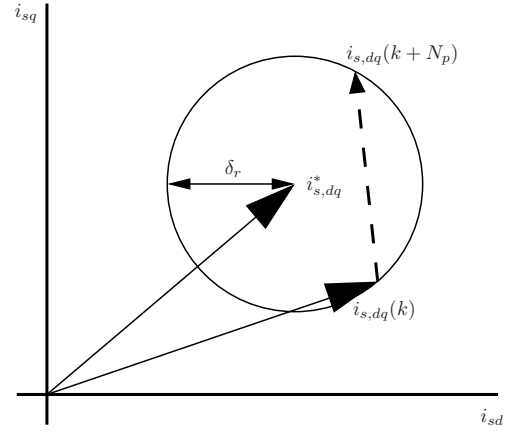(a) Boundary area and prediction process for MPDTC.
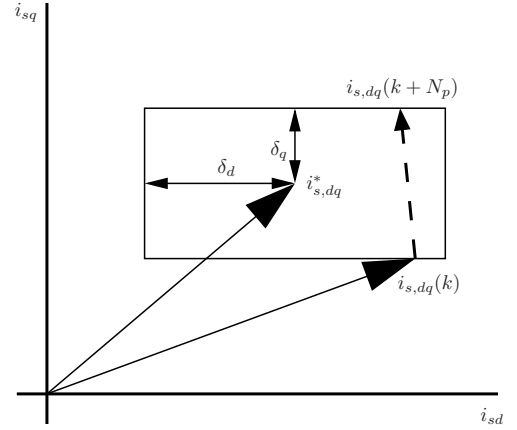
(b) Boundary area and prediction process for FMCC with a rectangular boundary.

Fig. 6: Comparison of the boundary areas and prediction sequences for MPDTC and FMCC-R on the dq-plane.

(a) Boundary area and prediction process for MPDCC.

(b) Boundary area and prediction process for FMCC with a circular boundary.

Fig. 7: Comparison of the boundary areas and prediction sequences for MPDCC and FMCC-C on the dq-plane.

sequence is one for which all of the output variables are either feasible, or pointing in the correct direction. An output variable is feasible if it lies within its hysteresis bounds. Pointing in the correct direction denotes the instance where an output variable lies outside the bounds, but moves closer to the reference at every time-step of the prediction horizon.

For a given switching horizon, each candidate sequence $U^i(k) = [u^i(k), u^i(k+1), ..., u^i(k + N_p^i - 1)]$, where $i \in \mathcal{I}$ and $\mathcal{I}$ is an index set, yields an associated cost which can be determined from

$$c^i = \frac{1}{N_p^i} \sum_{\ell=k}^{k+N_p^i-1} \|u^i(\ell) - u^i(\ell-1)\|_1 \qquad (23)$$

for minimisation of switching frequency, or

$$c^i = \frac{E^i}{N_p^i} \qquad (24)$$

for minimisation of switching losses, where E is the total switching energy loss over the prediction horizon. A detailed description of the calculation of switching losses is given in

[6]. The switching sequence $U^i(k)$ with the minimal cost is subsequently determined

$$i = \arg\min_{i \in \mathcal{I}} c^i. \qquad (25)$$

with the switching state $u(k) = u^i(k)$ applied. The horizon is subsequently shifted one step forward, with the process repeated at $k+1$. In addition to illustrating the hysteresis bounds, Figs. 6(a) and 7(a) show prediction sequences for MPDTC and MPDCC for a switching horizon of 'eSESESE'. References [6], [7] and [9] provide further details on the control procedure.

B. Forced Machine Current Control (FMCC)

Unlike MPDCC, where the switching horizon is variable and can be made up of a variety of 'S' and 'E' elements, the switching horizon for FMCC is effectively limited to 'SE', thus restricting the length of the prediction horizon. The control procedure for FMCC is similar to that of MPDxC. At each time-step k the stator current of the machine is sampled, and any intersection of the output trajectory with the boundary area

(a) FMCC-R (∘) and MPDTC: eSE (+). (b) FMCC-R (∘) and MPDTC: eSESESE (+). (c) PWM (▽), SVM (□), and OPP (⋆).

(d) FMCC-R (∘) and MPDTC: eSE (+). (e) FMCC-R (∘) and MPDTC: eSESESE (+). (f) PWM (▽), SVM (□), and OPP (⋆).
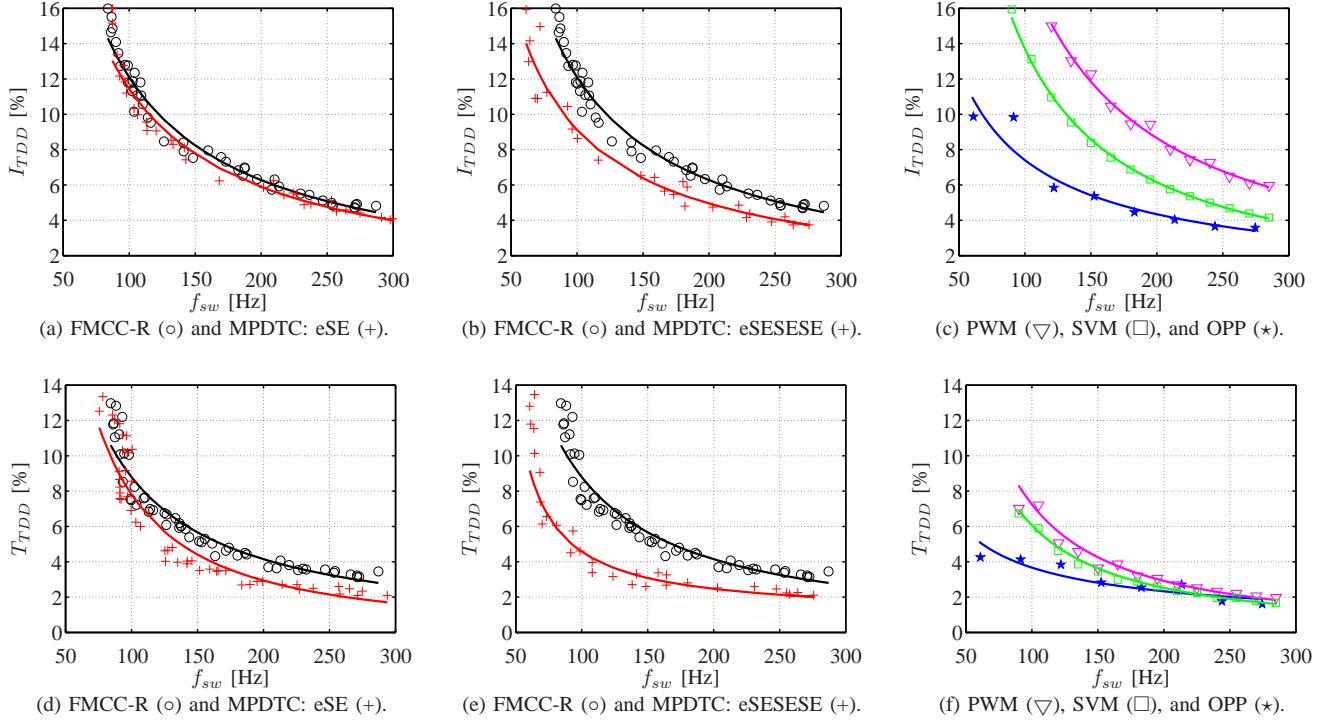
Fig. 8: Stator current and electromagnetic torque distortion against device switching frequency for FMCC-R, MPDTC, PWM, SVM and OPP.

detected. When an intersection is detected, when the output vector lies outside the boundary area, the set of allowable switching states which can be applied to the inverter at time-step k is determined based on the current switching state $u(k - 1)$. For each switching state which can be applied at time-step k, the trajectory of the outputs is extended forward in time using a linear extrapolation technique as described in [17] - [19]. During extension, the switching state is held constant until another intersection of the boundary area occurs. Each candidate switching state $u^i(k)$ will yield a prediction horizon of length N_p^i, where N_p is the number of time-steps from the switching time-step k to the next intersection of the boundary. Since FMCC minimises the switching frequency of the inverter, the cost associated with each switching state can be determined from (23) with the optimal state being that which minimises (25).

Along with showing the hysteresis bounds, Figs. 6(b) and 7(b) illustrate output predictions for FMCC-R and FMCC-C. At time-step k switching is necessitated due to the output current intersecting the boundary circle. The trajectory of the output current is predicted for the candidate switching state $u(k)$, with extension of the current trajectory resulting in a prediction horizon of length N_p.

In [19], Holtz and Stadtfeld proposed a method of optimisation by double prediction, where the controller preemptively selects a new switching state in order to avoid intersection of the boundary. This has the benefit of enforcing strict observance of the output bounds, as is the case for MPDxC with a horizon of the form 'eS...E'.

TABLE I: Rated values (left) and parameters (right) of the drive model used in simulations.

Induction Motor			
Voltage	3300 V	r_s	0.0108 p.u.
Current	356 A	r_r	0.0091 p.u.
Real power	1.587 MW	x_{ls}	0.1493 p.u.
Apparent power	2.035 MVA	x_{lr}	0.1104 p.u.
Frequency	50 Hz	x_m	2.3489 p.u.
Rotational speed	596 rpm		
Inverter			
DC-link voltage	5200 V	V_{dc}	1.930 p.u.

VI. PERFORMANCE EVALUATION

This section examines the performance of MPDxC and FMCC based on simulations carried out using the drive system outlined in Sect. II. A 3.3 kV, 50 Hz, 2 MVA squirrel-cage IM has been used as this is typical of machines used in the MV drive industry. The three-level NPC inverter has a total nominal DC-link voltage of 5.2 kV. ABB's 35L4510 4.5 kV 4 kA Integrated Gate Commutated Thyristor (IGCT) and 10H4520 fast recovery diode have been used for semiconductor devices. A summary of the machine and inverter parameters can be found in Table I. The p.u. system uses base values of $V_B = \sqrt{2/3}V_{rat} = 2694$ V, $I_B = \sqrt{2}I_{rat} = 504$ A, and $f_B = f_{rat} = 50$ Hz.

Simulations were run at 60% speed and full torque at steady state. In order to gauge the performance of MPDxC and FMCC, the performance of carrier-based PWM, SVM, and OPP have been included for comparison, which have been used for benchmarking in previous papers on MPDxC in [9] and [10]. The PWM scheme which has been used is carrier-based PWM with Phase-Disposition (PD) and a
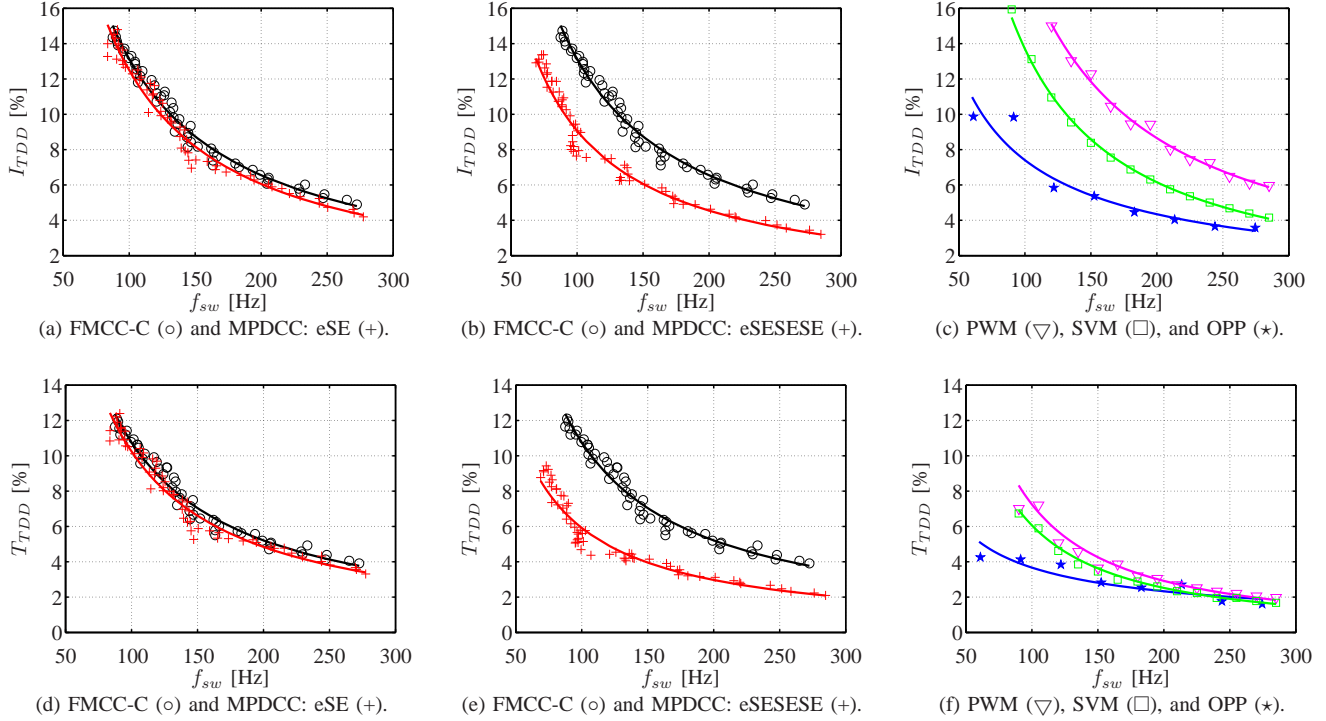
Fig. 9: Stator current and electromagnetic torque distortion against device switching frequency for FMCC-C, MPDCC, PWM, SVM and OPP.

min/max common-mode component added to the reference voltage. SVM has been implemented in the same manner as the PWM scheme, with the addition of a modulus operation to the common-mode component. As shown in [24], this is equivalent to conventional SVM, as both methods yield the same gating signals. The OPPs are calculated offline, and minimise the current distortion for a given pulse number (switching frequency) through optimisation of the switching angles for all possible operating points over a quarter of a fundamental period.

All extension steps for MPDxC and FMCC utilise the internal control model, rather than a linear or quadratic extrapolation technique. Although FMCC was proposed with linear extrapolation in [17] - [19], the use of precise extension allows for a fairer comparison with MPDxC. For MPDxC, all simulations have been run with the cost function penalising switching frequency. Note that the average switching frequency, f_{sw}, is taken as the average device switching frequency.

It has been assumed that the controller delay is negligible. Although in a practical setting the computation time associated with MPDxC and FMCC would take the majority of a sampling period, an appropriate compensation strategy, as discussed in [8] and [25], can largely mitigate the effects of such a delay.

Fig. 8 shows trade off curves for MPDTC and FMCC-R. The data points and hyperbolic trendlines shown are those of the approximate envelope of a greater set of data points, which are generated by varying $\delta_{|\Psi_s|}$ and δ_{T_e} for MPDTC and δ_d and δ_q for FMCC-R. Figs. 8(a) and 8(d) show the current and torque distortion, respectively, against switching frequency

for MPDTC with a horizon of 'eSE' and FMCC-R. As can be seen, the two schemes yield very similar levels of current distortion across the range of switching frequencies shown, with MPDTC with a short horizon offering a marginally lower level of TDD than FMCC-R. However, FMCC-R yields a somewhat higher level of torque distortion. This can be explained by the fact that MPDTC switches in anticipation of the outputs intersecting the boundary, whereas FMCC-R switches after intersection has occurred. This widens the effective bounds of FMCC-R, which, in the case of q-axis stator current/flux, results in higher torque TDD.

Figs. 8(b) and 8(e) show the current and torque distortion for MPDTC with a long horizon of 'eSESESE' and FMCC-R. This highlights the impact of the longer switching horizon on distortion, with MPDTC showing a significant improvement over FMCC-R, with this being particularly evident at low switching frequencies. At 100 Hz, MPDTC with a long horizon offers a relative current TDD about 25% lower than FMCC-R, and a relative torque TDD about 50% lower.

Fig. 8(c) shows current distortion against switching frequency for PWM, SVM, and OPP. It is apparent that both FMCC-R and MPDTC with short and long horizons offer lower current distortion than PWM. SVM yields a slightly higher level of current distortion than FMCC-R and MPDTC with a short horizon at low frequencies, and a similar level of distortion above about 150 Hz. OPP yields a much lower level of distortion than the predictive schemes at low frequencies, however as the switching frequency increases, the difference between the schemes reduces.

Fig. 8(f) makes the same comparison for torque distortion.
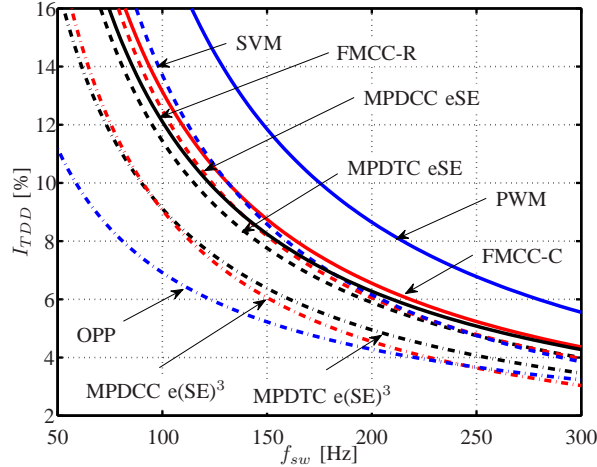
(a) Comparison of current distortion vs device switching frequency trade-off curves.
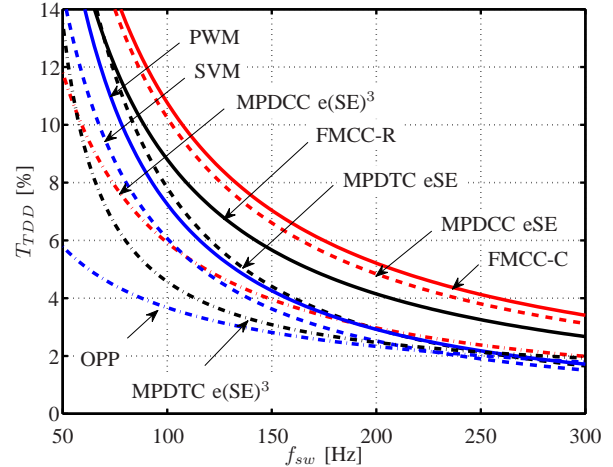
(b) Comparison of torque distortion vs device switching frequency trade-off curves.

Fig. 10: Performance trade off curves for FMCC, MPDxC, PWM, SVM and OPP.

PWM gives a similar level of distortion to MPDTC with a short horizon, while MPDTC with a long horizon offers a lower level of distortion than SVM. OPP yields the lowest distortion. As is the case for current distortion, as the switching frequency increases the trendlines begin to converge. With the exception of FMCC-R, little difference between the schemes is visible from 250 Hz onwards.

The trade-off curves of Fig. 9 show the current and torque TDD against switching frequency for MPDCC and FMCC-C, with the data points generated by varying δ_i and δ_r, respectively. Figs. 9(a) and 9(d) show the current and torque TDD against switching frequency for MPDCC with a horizon of 'eSE' and FMCC-C. It is evident that these schemes yield very similar levels of performance. However, MPDCC performs slightly better, which can be explained by the fact that, like MPDTC, MPDCC switches in anticipation of the outputs intersecting the boundary, whereas FMCC switches after intersection has occurred. Moreover, the hexagonal boundary area of MPDCC results in a constant and symmetrical ripple for each phase current, whereas the circular boundary of FMCC-C results in a non-constant ripple for each phase current and a slightly higher level of current and torque distortion. Figs. 9(b) and 9(e) show FMCC-C and MPDCC with the switching horizon extended to 'eSESESE'. The difference between the two is much more notable, with MPDCC showing a significant improvement in current and torque distortion across the full range of switching frequencies. At a switching frequency of 100 Hz, MPDCC with a long horizon offers a relative current TDD about 30% lower than FMCC-C, and a relative torque TDD about 45% lower.

Figs. 9(c) and 9(f) show the current and torque distortion of PWM, SVM and OPP. It is apparent that PWM results in a higher current distortion than the predictive schemes. SVM offers a similar current TDD to FMCC-C and MPDCC with a short horizon. OPP offers the lowest current distortion at most

frequencies, however at frequencies above 250 Hz the current distortion is similar to that of MPDCC with a long horizon. The relationship between the schemes is quite different in terms of torque. MPDCC with a short horizon and FMCC-C give a considerably poorer level of torque distortion than PWM. MPDCC with a long horizon yields a similar torque distortion to SVM at 100 Hz, but is slightly worse than SVM and similar to PWM above about 150 Hz.

It is interesting to note the nature of the PWM, SVM and OPP trendlines, as compared to those of the predictive schemes. For PWM and SVM, the data points are very nearly hyperbolic in nature, with the trendlines matching the points very closely. For OPP the hyperbolic trend is reasonably strong, although to a lesser extent than PWM/SVM. The predictive schemes on the other hand have much more scattered data sets; the hyperbolic trendlines describe the overall patterns well, but there is noticeable error between the trendline and the data points.

Fig. 10 summarises the current and torque distortion trade-off curves for MPDTC, MPDCC, FMCC-R, FMCC-C, PWM, SVM and OPP, with the device switching frequency ranging from 50 to 300 Hz. It is evident that FMCC-C has the highest level of current and torque distortion among the predictive schemes under investigation, while FMCC-R yields a similar current distortion, and lower torque distortion, than MPDCC with a short switching horizon. This seems surprising at first, since FMCC-R is a torque control scheme with bounds which are not designed to minimise current distortion. However, since FMCC-R possesses two tuning parameters compared to one for MPDCC, there are a large number of possible ratios between δ_d and δ_q, which means the envelope of the data points for current distortion is capable of matching that of MPDCC with a short horizon. However, it is important to note that in the case of MPDTC and FMCC-R, low current and torque distortion are not achieved simultaneously. The

TABLE II: Comparison of FMCC, MPDxC, PWM, SVM and OPP. Comparison is made at two points - the first column is at a current TDD of 6%, and the second column at a torque TDD of 4%. Values are shown in both absolute terms and relative to PWM.

Control scheme	Switching horizon	f_{sw} [Hz]	f_{sw} [%]	f_{sw} [Hz]	f_{sw} [%]
PWM	-	280	100	157	100
SVM	-	204	73	139	89
FMCC-R	SE	210	75	207	132
MPDTC	eSE	196	70	161	103
MPDTC	eSESESE	161	58	113	72
FMCC-C	SE	218	78	258	164
MPDCC	eSE	202	72	239	152
MPDCC	eSESESE	151	54	148	94
OPP	-	123	44	88	56

points which constitute the envelope for current distortion, each of which corresponds to a particular tuning of $\delta_{|\Psi_s|}$ and δ_{T_e}, or δ_d or δ_q, are not the same as those which make up the envelope for torque distortion; in order for MPDTC and FMCC-R to achieve low torque TDD at a given switching frequency, current TDD may be sacrificed, and vice versa. Like FMCC-C, FMCC-R results in a higher level of current and torque distortion than MPDCC with a long horizon, which is particularly noticeable at lower frequencies.

The performances of the control schemes under consideration tend to converge as the switching frequency increases. This is most prominent in the case of torque distortion where, with the exception of FMCC-R, FMCC-C, and MPDCC with a short horizon, the schemes tend to converge around the OPP trade-off curve. Table II summarises the switching frequency of the schemes relative to PWM at two points - the first column is at a current TDD of 6%, and the second at a torque TDD of 4%.

Although all comparisons have been made at 0.6 p.u. speed, it is expected that the performance of MPDTC relative to FMCC-R, and MPDCC relative to FMCC-C, would remain similar at full-rated speed. However, at rated speed, the performance difference *between* the torque and current schemes may differ; while the performance of MPDTC relative to FMCC-R will be similar at full speed, the performance of MPDTC relative to MPDCC may be quite different. Moreover, by changing the speed, the performance of the predictive schemes may change relative to PWM, SVM and OPP.

As has been previously stated in Sect. I, all simulations have been carried out under the assumption of a fixed neutral point. This is due to the fact that FMCC was initially proposed for a two-level converter, meaning neutral point balancing is not mentioned in early literature. The issue of neutral point balancing has been addressed for MPDxC in [7] and [9]. By defining a set of hysteresis bounds around the neutral point reference (zero), and expanding the internal control model to capture the dynamics of the neutral point, the neutral point potential can be treated as an additional output variable. The inclusion of a floating neutral point has been shown to slightly degrade the *absolute* performance of MPDTC and MPDCC, however, the *relative* performance of the schemes remains almost the same. Because of the similarities between MPDxC and FMCC, the technique as discussed in [7] and [9] could easily be applied to FMCC. As has been observed for MPDxC, this would result in a slight decrease in the absolute performance of FMCC. However, the relative performance between MPDxC and FMCC would remain nearly constant.

VII. CONCLUSION

This paper has presented a review and comparison of two predictive control methodologies: MPDxC and FMCC. A summary of the drive system and corresponding internal models used by the controllers have been presented. The hysteresis bounds which are used by the controllers were discussed and the control procedures were summarised.

Through simulation of a three-level NPC inverter driving a MV induction motor, FMCC-R and FMCC-C have been shown to perform to similar levels as MPDTC and MPDCC with short switching horizons. FMCC-R has been shown to be capable of better performance than FMCC-C and MPDCC with a short horizon in terms of torque distortion. Moreover, FMCC-R has been shown to be capable of matching the performance of MPDCC with a short horizon in terms of current distortion. However, like MPDTC, it does not necessarily yield low current and torque TDD simultaneously.

Comparison has been made at a fixed speed of 0.6 p.u. with full torque, which is a typical operating condition for a MV drive. Additionally, the neutral point potential has been assumed to be fixed. While inclusion of a floating neutral point would slightly worsen the absolute performance of the schemes, it is expected that their relative performance would remain very similar.

For MV drives, the benefit of predictive control schemes lies in their ability to reduce converter switching frequency with respect to traditional FOC while maintaining acceptable levels of harmonic distortion, or vice versa. At switching frequencies below 150 Hz, MPDTC and MPDCC with long horizons are clearly the best among the predictive controllers in terms of both current and torque distortion. However, at higher switching frequencies in the range of 200 – 300 Hz, the margin between long horizon MPDxC, and FMCC/short horizon MPDxC, is less pronounced.

REFERENCES

[1] D. Q. Mayne, J. B. Rawlings, C. V. Rao, and P. O. M. Scokaert, "Constrained model predictive control: Stability and optimality," *Automatica*, vol. 36, no. 6, pp. 789–814, Jun. 2000.

[2] S. J. Qin and T. A. Badgwell, "A survey of industrial model predictive control technology," *Control Eng. Pract.*, vol. 11, no. 7, pp. 733–764, Jul. 2003.

[3] A. Linder and R. Kennel, "Model predictive control for electrical drives," in *Proc. IEEE Power Electron. Spec. Conf.*, Recife, Brasil, Jun. 2005.

[4] S. Mariethoz, A. Domahidi, and M. Morari, "Sensorless explicit model predictive control of permanent magnet synchronous motors," in *Proc. IEEE Int. Elect. Mach. Drives Conf.*, Miami, USA, May 2009.

[5] T. Geyer, "Low complexity model predictive control in power electronics and power systems," Ph.D. dissertation, Automatic Control Laboratory, ETH Zurich, 2005.

[6] T. Geyer, "Generalized model predictive direct torque control: Long prediction horizons and minimization of switching losses," in *Proc. IEEE Conf. Decis. Control*, Shanghai, China, Dec. 2009.

[7] T. Geyer, G. Papafotiou, and M. Morari, "Model predictive direct torque control - part I: Concept, algorithm and analysis," *IEEE Trans. Ind. Electron.*, vol. 56, no. 6, pp. 1894–1905, Jun. 2009.

[8] G. Papafotiou, J. Kley, K. Papadopoulos, P. Bohren, and M. Morari, "Model predictive direct torque control - part II: Implementation and experimental evaluation," *IEEE Trans. Ind. Electron.*, vol. 56, no. 6, pp. 1906–1915, Jun. 2009.

[9] T. Geyer, "Model predictive direct current control: Formulation of the stator current bounds and the concept of the switching horizon," *IEEE Ind. Appl. Mag.*, vol. 18, no. 2, pp. 47–59, Mar. 2012.

[10] T. Geyer, "A comparison of control and modulation schemes for medium-voltage drives: Emerging predictive control concepts versus PWM-based schemes," *IEEE Trans. Ind. Appl.*, vol. 47, no. 3, pp. 1380–1389, May/Jun. 2011.

[11] J. C. Ramirez Martinez, R. M. Kennel, and T. Geyer, "Model predictive direct current control," in *Proc. IEEE Int. Conf. Ind. Technol.*, Vina del Mar, Chile, Mar. 2010.

[12] J. Rodriguez, J. Pontt, C. Silva, P. Cortes, U. Amman, and S. Rees, "Predictive current control of a voltage source inverter," *IEEE Trans. Ind. Electron.*, vol. 54, no. 1, pp. 495–503, Feb. 2007.

[13] R. Vargas, P. Cortes, U. Ammann, J. Rodriguez, and J. Pontt, "Predictive control of a three-phase neutral-point-clamped inverter," *IEEE Trans. Ind. Electron.*, vol. 54, no. 5, pp. 2697–2705, Oct. 2007.

[14] P. Cortes, M. P. Kazmierkowski, R. M. Kennel, D. E. Quevedo, and J. Rodriguez, "Predictive control in power electronics and drives," *IEEE Trans. Ind. Electron.*, vol. 55, no. 12, pp. 4312–4324, Dec. 2008.

[15] S. Kouro, P. Cortes, R. Vargas, U. Ammann, and J. Rodriguez, "Model predictive control - a simple and powerful method to control power converters," *IEEE Trans. Ind. Electron.*, vol. 56, no. 6, pp. 1826–1838, Jun. 2009.

[16] H. Miranda, P. Cortes, J. Yuz, and J. Rodriguez, "Predictive torque control of induction machines based on state-space models," *IEEE Trans. Ind. Electron.*, vol. 56, no. 6, pp. 1916–1924, Jun. 2009.

[17] J. Holtz and S. Stadtfeld, "A predictive controller for the stator current vector of AC machines fed from a switched voltage source," in *Proc. Int. Power Electron. Conf.*, Tokyo, Japan, 1983.

[18] J. Holtz and S. Stadtfeld, "Field-oriented control by forced motor currents in a voltage fed inverter drive," in *Proc. IFAC Symp. Control in Power Electron. and Elect. Drives*, Lausanne, Switzerland, Sep. 1983.

[19] J. Holtz and S. Stadtfeld, "A PWM inverter drive system with on-line optimized pulse patterns," in *Proc. Eur. Conf. Power Electron. Appl.*, Brussels, Belgium, Oct. 1985.

[20] A. Khambadkone and J. Holtz, "Low switching frequency and high dynamic pulsewidth modulation based on field-orientation for high-power inverter drive," *IEEE Trans. Power Electron.*, vol. 7, no. 4, pp. 627–632, Oct. 1992.

[21] T. Geyer, "Computationally efficient model predictive direct torque control," *IEEE Trans. Power Electron.*, vol. 26, no. 10, pp. 2804–2816, Oct. 2011.

[22] P. C. Krause, O. Wasynczuk, and S. D. Sudhoff, *Analysis of Electric Machinery and Drive Systems*, 2nd ed. New York: Wiley, 2002.

[23] Y. Zeinaly, T. Geyer, and B. Egardt, "Trajectory extension methods for model predictive direct torque control," in *Proc. IEEE Appl. Power Electron. Conf. Expo.*, Fort Worth, USA, Mar. 2011.

[24] B. P. McGrath, D. G. Holmes, and T. Lipo, "Optimized space vector switching sequences for multilevel inverters," *IEEE Trans. Power Electron.*, vol. 18, no. 6, pp. 1293–1301, Nov. 2003.

[25] P. Cortes, J. Rodriguez, C. Silva, and A. Flores, "Delay compensation in model predictive current control of a three-phase inverter," *IEEE Trans. Ind. Electron.*, vol. 59, no. 2, pp. 1323–1325, Feb. 2012.

James Scoltock (S'10) graduated with the BE(Hons) degree in electrical and electronic engineering from The University of Auckland, New Zealand, in 2010. He is currently a PhD candidate at the same university. His research interests are in the areas of power electronics and model predictive control.

Tobias Geyer (M'08–SM'10) received the Dipl.-Ing. and Ph.D. degrees in electrical engineering from ETH Zurich, Zurich, Switzerland, in 2000 and 2005, respectively.

From 2006 to 2008, he was with the High Power Electronics Group of GE's Global Research Centre, Munich, Germany, where he focused on control and modulation schemes for large electrical drives. Subsequently, he spent three years at the Department of Electrical and Computer Engineering, The University of Auckland, Auckland, New Zealand, where he developed model predictive control schemes for medium-voltage drives. In 2012, he joined ABB's Corporate Research Centre, in Baden, Switzerland.

Dr. Geyer's research interests are at the intersection of power electronics, modern control theory and mathematical optimization. This includes model predictive control and medium-voltage electrical drives. He was a recipient of the Second Prize Paper Award at the 2008 IEEE Industry Applications Society Meeting. He serves as an associate editor of the Industrial Drives Committee of the Transactions on Industry Applications.

Udaya K. Madawala (M'93–SM'06) graduated with B.Sc. (Electrical Engineering)(Hons) from The University of Moratuwa, Sri Lanka in 1987 and received his PhD (Power Electronics) from The University of Auckland, New Zealand in 1993.

After working in industry, he joined the Department of Electrical and Computer Engineering at The University of Auckland in 1997, where he presently works as an Associate Professor. His research interests are in the fields of power electronics, inductive power transfer and renewable energy, and is a consultant to industry.

Dr. Madawala is an active IEEE volunteer and serves as an Associate Editor for both IEEE Transactions on Industrial Electronics and Power Electronics. He is a member of the Power Electronics Technical Committee and also the Chairman of the Joint Chapter of IEEE Industrial Electronics Society and Industrial Applications Society in New Zealand (North).